Chapter

Synthesis of Nano-Composites Mg_2TiO_4 Powders via Mechanical Alloying Method and Characterization

Ranjan Kumar Bhuyan, Bhagban Kisan, Santosh Kumar Parida, Soumya Patra and Sunil Kumar

Abstract

In this chapter a systematic investigation of impact of mechanical activation on structural, microstructural, thermal and optical properties of MgO – TiO_2 nanocrystalline composite system, synthesized via high energy ball milling techniques. Williamson-Hall (W-H) plot method was employed to understand the signature of the broadening in the XRD peaks and for the estimation of crystallite size of MgO – TiO_2 nanocrystalline composite system. It revealed that the peak broadening is not only due to reduced coherently diffracting domain size but also due to a significant strain distribution. The calculated strain was 9.01×10^{-3} and the average crystallite sizes were 40–60 nm for 35 hours (hrs) milled powder and this result is very much consistent with transmission electron microscopy (TEM) analysis. The SAED ring pattern indicates that the phase of Mg_2TiO_4 - nanoparticles was polycrystalline in structure and the distance between crystalline planes was consistent with the standard pattern for a spinel Mg_2TiO_4 crystal structure. To analyze the lattice fringes for the 35 hrs milled samples high resolution-TEM (HR-TEM) study was carried out and the result revealed that the each particle has single crystalline structure. Morphological studies were carried out by using SEM analysis. The thermal decomposition behavior of the milled powders was examined by a thermogravimetric analyzer (TGA) in argon atmosphere. Also, MTO nanoparticles showed a strong absorption at ~356 nm and the band gap values ranged between 3.26-3.78 eV with an increase of milling time from 0 to 35 hr. The mechanically derived MTO nanoparticles showed promising optical properties which are suitable for commercial optoelectronic applications.

Keywords: high energy ball milling, MgO – TiO_2 composite system, W-H method, microstructure, TEM and HR- TEM, DSC-TGA analysis, optical studies

1. Introduction

The tremendous growth in telecommunication industries has led increasing demand on the development of low loss and low cost high frequency dielectric ceramics in the form of resonators, filters, antennas, substrates [1–4]. Moreover, the recent demand has focused on searching for low loss materials with lower

permittivity to miniaturize the devices [4–7]. This is because low permittivity can not only reduce cross coupling with conductors but also precise the time for the transmission of electronic signal. Moreover, due to extension of carrier frequency high-quality factor ($Q \times f_o$) and nearly zero temperature coefficient of resonant frequency (τ_f) also play crucial roles for frequency selectivity and temperature stability of the system, respectively [5–10]. Various smart electronic materials were proposed to fulfill these requirements for high-frequency applications [5–13]. Recently, searching for low loss dielectric ceramics based on MgO - TiO_2 binary system has brought much more attention. It was reported that MgO – TiO_2 system has three stable phases, such as $MgTiO_3$, Mg_2TiO_4 and $MgTi_2O_5$ [14, 15], which are used for microwave engineering/RF- applications. These binary magnesium titanates ($MgTiO_3$, Mg_2TiO_4 and $MgTi_2O_5$) are differed extremely from other materials due to their good dielectric properties. It has been established that $MgTiO_3$ possesses ilmenite structure, $MgTi_2O_5$ has pseudobrookite structure and Mg_2TiO_4 has an inverse spinel structure belonging to cubic space group of Fd3m (227) [16, 17]. Out of them magnesium orthotitanate (Mg_2TiO_4) is a promising dielectric material with excellent microwave dielectric properties, i.e., medium dielectric constant (ε_r) ~ 14, high-quality factor ($Q \times f_o$) ~150,000 GHz and a negative temperature coefficient of resonant frequency (τ_f) ~ – 50 ppm/^oC [15].

Ceramic nonmaterials have great scientific interest due to their unique physical and chemical properties and are significantly different from bulk counterparts. A bulk material has fixed physical properties regardless of its size, but reducing the particle size into nanoscale, by keeping chemical composition fixed, can change the fundamental properties of the materials [18]. A unique aspect of nanoscale materials is that they have large surface area to volume ratio, which opens new possibilities of surface dependent phenomena that are practically very useful for various applications. As the size of the material decreases into the nanoscale dimensions (less than 100-200 nm), a number of physical phenomena have come into notice, which drove our attention for the synthesis of nanocrystalline - Mg_2TiO_4 powders. There are very few papers are available about the effect of mechanical activation on MgO - TiO_2 binary system and to investigate its physical changes. Recently, Bhuyan et al., [19], have studied the influence of high energy ball milling on structural, microstructural and optical properties of Mg_2TiO_4 nanoparticles. They proposed that MTO nanoparticles prepared by mechanical alloying method exhibited promising optical properties which are suitable for commercial optoelectronic applications. In another study, Bhuyan et al., [20], have studied the structural and microwave dielectric properties of Mg_2TiO_4 ceramics synthesized by mechanical alloying method. Cheng et al. [21], have investigated the microwave dielectric properties of Mg_2TiO_4 ceramics synthesized via high energy ball milling method. Filipovic et al., [22], have studied the influence of mechanical activation on microstructure and crystal structure of sintered MgO-TiO_2 system.

In this present chapter, Mg_2TiO_4 (MTO) nano-composite ceramics were synthesized via mechanical alloying (MA) method with the help of high energy planetary ball milling. Mechanical alloying is a most efficient, cost effective and convenient method for the synthesis of a wide range of nanosized metallic and ceramic powders [23]. This method has many advantages such as simplicity, relatively inexpensive compared to other techniques to produce large scale nanoparticles and can be applicable to any type of materials [24]. The most important merit of this technique is that the solid-state reaction is activated via mechanical energy rather than production of heating energy. Moreover, mechanically synthesized powders have good physical properties than those derived by a conventional solid-state reaction and most of the wet-chemical processes [25]. Mechanical synthesis not only makes the material finer but also includes structural changes, phase transformations and

even solid-state reactions among the solid reagents. These physicochemical changes occur due to the efficient transformation of the mechanical energy of the grinding media to the particles and the intensive mechanical force during the milling process [26].

It is well known that a perfect crystal would extend in all possible directions to infinity; however, no such crystals are perfect due to their finite size. This deviation from its perfect crystallinity is the main cause for broadening of the X-ray diffraction peaks of materials. There are two important characteristics extracted from the peak width analysis viz. crystallite size and lattice strain. Crystallite size is a measure of the size of a coherently diffracting domain whereas lattice strain is a measure of the distribution of lattice constants arising from crystal imperfections, such as lattice dislocation. The other sources of strain are the grain boundary triple junctions, crystal imperfections, contact or sinter stresses, stacking faults etc. [26]. The X-ray line broadening is used for the investigation of dislocation distribution. Moreover, it should be noted that crystallite size of the particles is not same as the particle size due to the presence of polycrystalline aggregates. The particle size can be measured from various techniques such as scanning electron microscope (SEM) or field emission scanning electron microscope (FE-SEM) and transmission electron microscope (TEM) analysis. Various methods are adopted by different researchers for the estimation of crystallite size and lattice strain, which are X-ray peak profile analysis (XPPA), pseudo-Voigt function, Rietveld refinement, and Warren-Averbach analysis [27–29]. However, in the present study, Williamson–Hall (W–H) method is a simplified integral breadth method employed for the determination of crystallite size and lattice strain, by considering the peak width as a function of 2θ [30].

In this chapter, the impact of mechanical activation of the MgO-TiO_2 system for the synthesis of nanocrystalline Mg_2TiO_4 powders via high energy ball milling technique has been investigated. The effect of milling time on crystal structure, microstructure, thermal and optical properties of this proposed system is being studied. This study further reveals the importance of W- H method for the determination of crystallite size and lattice strains.

2. Experimental details

2.1 Materials

The Mg_2TiO_4 powders were prepared from commercially available high- purity oxides MgO (99.99% purity) and TiO_2 (99.99% purity) of Sigma Aldrich (St.Louis, MO), as starting materials.

2.2 Synthesis of Mg_2TiO_4 nano-composite alloys

In this chapter, high energy planetary ball milling techniques was used for the synthesis of Mg_2TiO_4 nano-composite alloys from high- purity MgO and TiO_2 oxides. The starting materials were weighted according to desired stoichiometry ratios and milled for 5 – 35 hrs to reach steady state condition using planetary ball mill (Fritsch, GmBH, Germany) with the following parameters: (i) ball-to-powder ratio: 10:1; ball diameter: 8 and 16 mm; ball and vial materials: harden stainless steel; the vial rotation speed: 350 rpm. In order to avoid significant temperature rise, the milling process was stopped periodically for every 10 minutes and then resumed for 5 minutes. A brief description about the ball milling techniques is summarized below.

Ball milling technique: The photographic view of planetary ball mill is depicted by **Figure 1(a)** and in **Figure 1(b)** it is shown the Zirconia jars with zirconia balls. The zirconia balls are selected in order to avoid the contamination with the given sample. The vials mounted on the horizontal disc rotate in a direction opposite to that of the disc and thereby simulating a planetary-like motion (as shown in **Figure 2**). This result in large outward force acting on the balls kept inside the vial and causes the balls to collide with them and also to the wall of the vial more energetically. When the Mg_2TiO_4 oxide powders are kept inside the vial along with the balls, the powders undergoes repeated cold welding and fracture at the surfaces of the balls and the vial. This process leads to disintegration of the powders, resulting first in refinement of crystallite size to produce nanocrystalline alloys along with a large number of defects in the parent powders [26, 31–33]. Hence, crystallite size refinement is a natural consequence of a ball milling process. As the milling time progresses the alloy becomes amorphous. The refinement and alloying processes are estimated by the milling parameters including ball to powder weight ratio, size of the ball, speed of rotation, duration of milling etc. Moreover, the nature of the milling container (or vial), milling media and types of balls used during the milling process also played an important role in synthesizing nanocrystalline powders [34].

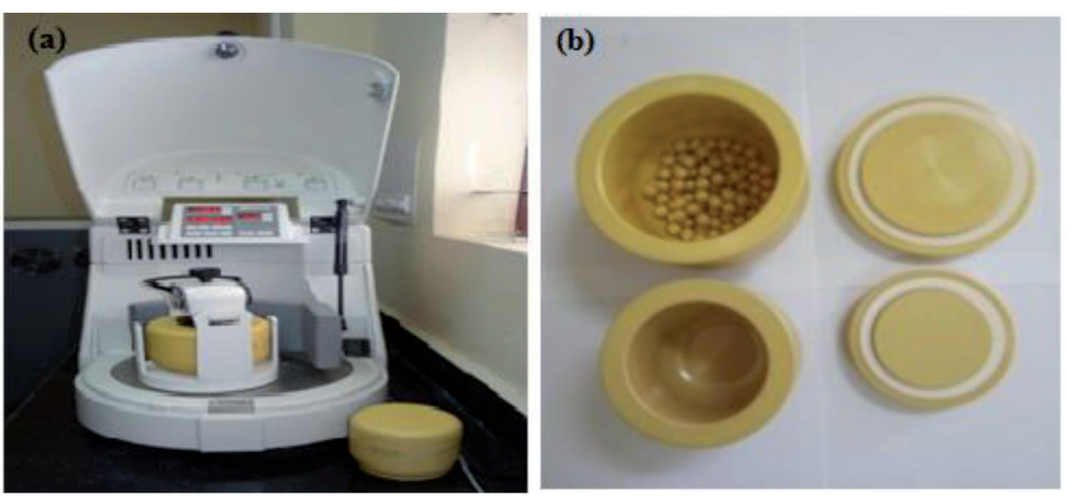

Figure 1.
(a) Photographic view of planetary ball mill (b) zirconia jar with zirconia balls.

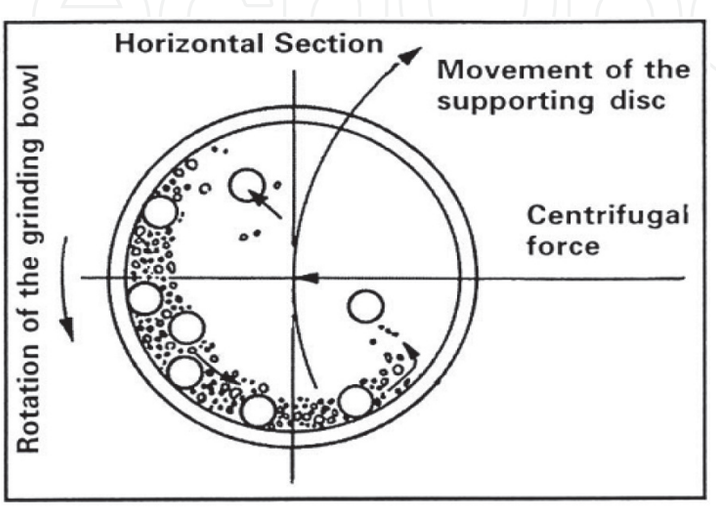

Figure 2.
Schematic diagram of the horizontal section of a vial depicting the movement of the balls inside the vial due to its planet like movement [26].

2.3 Characterizations techniques

Room temperature X-Ray diffraction (XRD) analysis was carried out to determine the crystallite size, lattice strain, lattice parameter and phase analysis of the different hours milled powder sample using X-ray Diffractometer (Rigaku TTRAX 18 KW CuK_α radiation). Recording of microstructure of 35 hrs nanocrystalline Mg_2TiO_4 milled powders has been carried out by using transmission electron microscope (TEM, JEOL 2100; JEOL, Tokyo, Japan). The surface morphology of nanocrystalline Mg_2TiO_4 milled powders was observed by scanning electron microscopy (SEM, Leo 1430, PV, Carl Zeiss Jena, Germany). The thermal decomposition behavior of the different hours milled powders was examined by a thermogravimetric analyzer (TGA, NETZSCH, STA 449-F3. Jupiter) at a heating rate of 10°C/min in the argon atmosphere. UV–VIS–NIR spectrophotometer (UV 3101PC, Shimdzu) was used to obtained UV/VIS absorption spectra of all the samples in the wavelength range 200–1000 nm.

3. Results and discussion

3.1 Structural properties

X-ray diffraction (XRD) patterns of prepared Mg_2TiO_4 nanoparticles milled for different hours via high energy ball milling was taken and is illustrated in **Figure 3**. XRD patterns indicates that for the samples milled for 5 hrs exhibited the peaks corresponding to initial compounds MgO and TiO_2 only. When the milling time increases, the intensities of the parent oxide peaks appear to be depressed gradually and the formation of associated $MgTi_2O_5$ phase was observed. When the milling time increased to 30 hrs, all the starting oxides peaks are disappeared completely. At the same time high intense diffraction peaks of pure- Mg_2TiO_4 phase are observed with small significance of $MgTiO_3$ and $MgTi_2O_5$ phases. However, when the milling time reached to 35 hrs, the

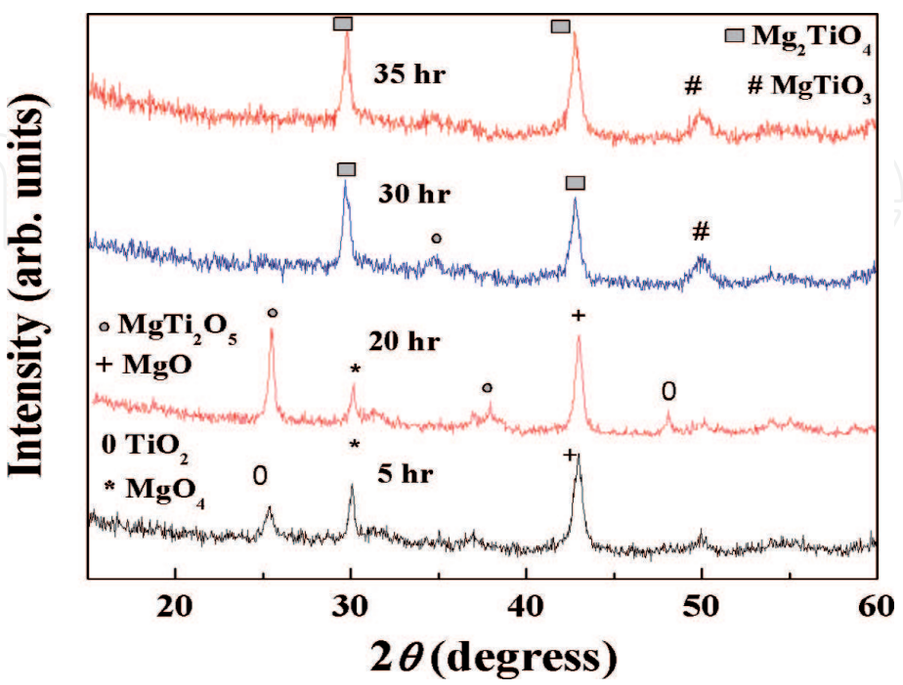

Figure 3.
XRD patterns of the MgO and TiO_2 oxides milled for 5, 20, 30 and 35 hrs (adapted with permission from Bhuyan et al., 2020, @ Springer *[19]).*

sample showed more intensified Mg_2TiO_4 phases along with small $MgTiO_3$ peak. This signifies that crystallite nature of pure Mg_2TiO_4 sample enhances and is confirmed from ICSD – PDF # 06–5792. The presence of associated phases such as $MgTi_2O_5$ and $MgTiO_3$ in the MgO - TiO_2 system is mostly due to the difference in the degree of the incipient mechanical reaction. This can be explained as follows: at the time of milling, the mechanical energy of the grinding media transforms into the given oxide particles that causes structural destruction followed by reduction in particle size [26].

3.2 Williamson - Hall (W - H) method

The crystallite size of nanoparticles can be determined with several techniques that rely upon the peak width of the X - ray diffraction patterns. In the present study, Williamson-Hall (W-H) plot method as well as Scherrer formula have been chosen in order to understand the origin of the broadening in the XRD peak.

The broadening of XRD peaks is due to crystallite size and strain contributions. The average crystallite size was calculated from XRD peak width based on Debye–Scherrer's equation,

$$D = \frac{k\lambda}{\beta_{\text{hkl}} \cos\theta} \tag{1}$$

where β_{hkl} is the full width half maximum, D is the crystallite size, k is the shape factor which is taken as 0.9 for spherical particles, λ is the wavelength of incident X-ray radiation (λ = 0.154 nm for Cu-K_α) and θ is the Bragg angle of the analyzed peaks.

According to Williamson and Hall, the strain-induced broadening in nanocrystalline powders due to crystal imperfection and distortion was calculated using the formula [35],

$$\varepsilon = \frac{\beta_{\text{hkl}}}{4\tan\theta} \tag{2}$$

Here, ε is the effective strain associated with mechanical alloying. Now, the total peak broadening is defined as the sum of the contributions of crystallite size and strain present in the material and can be expressed as [36],

$$\beta_{\text{hkl}} = \beta_D + \beta_\varepsilon \tag{3}$$

where β_D is due to the contribution of crystallite size, β_ε is due to strain-induced broadening and β_{hkl} is the width of the half-maximum intensity of instrumental corrected broadening. This β_{hkl} can be calculated by using the relation,

$$\beta_{hkl} = \left[\left(\beta^2{}_{hkl}\right)Measured - \left(\beta^2{}_{hkl}\right)Instrumental\right]^{1/2} \tag{4}$$

If we consider the particle size and strain contributions to line broadening are independent to each other and both have a Cauchy-like profile, then the observed line breadth is the sum of Eqs. (1) and (2) and is given by [35],

$$\beta_{\text{hkl}} = \left[\frac{k\lambda}{D\cos\theta}\right] + 4\varepsilon\sin\theta \tag{5}$$

By rearranging the above equation, we get,

$$\beta_{\text{hkl}}\cos\theta = \left[\frac{k\lambda}{D}\right] + 4\varepsilon\sin\theta \tag{6}$$

This is the Williamson- Hall equation, which represents the uniform deformation model. The average crystallite size is estimated for selected peaks of nanocrystalline MTO powders milled for different hours by using Eqs. (1) and (6). The variation of average crystallite size as a function of milling time calculated by both the method is plotted and is depicted in **Figure 4 (a)**. It is clear from **Figure 4(a)** that up to 30 hrs of milling the average crystallite size decreases sharply and then attains a constant value. The average crystallite size of the parent sample was found to be nearly 2.5 μm. But for 20 hrs of milling, the crystallite size reduced to 100-120 nm and for 35 hrs of milling it becomes 40-60 nm, as calculated by W-H method. From Scherer formula the average crystallite size for MTO powder are found to be 28 nm and 17 nm, respectively after 20 and 35 hrs of milling. Thus the crystallite size calculated from the Scherer equation is smaller than that of the W-H method. This is due to the fact that the Scherer's equation does not account for the lattice strain effect that causes line broadening.

Mg_2TiO_4 has an inverse spinel structure and having structural formula $Mg[\mathrm{MgTi}]O_4$ and belonging to the cubic space group of Fd3m (227) [15]. The Ti and Mg atoms occupy the tetrahedral (8a) and octahedral (16d) sites and the oxygen atoms are in (32e) site symmetry position [20]. According to Bragg's law [37],

$$2d\sin\theta = n\lambda \tag{7}$$

where, n is the order of diffraction and it is usually taken as $n = 1$, λ is the wavelength of incident X-ray and d is the spacing between parallel planes of given miller indices *h, k and l*. Since, Mg_2TiO_4 has cubic structure, so the lattice constants are $a = b = c$. The d-spacing is related to the lattice constant a, and the miller indices *h, k and l*, by the following relation [37],

$$d = \frac{a}{\sqrt{h^2 + k^2 + l^2}} \tag{8}$$

By using Eq. (7), the lattice constant of selected planes is calculated by following relation,

$$a = \frac{\lambda}{2\sin\theta}\sqrt{h^2 + k^2 + l^2} \tag{9}$$

The variation of lattice parameter as a function of different milling time is plotted and is illustrated as inset **Figure 4(a)**. The results showed that the lattice constant decreases with increase of milling time from 8.436 Å to a stable value of 8.412 Å. This difference in lattice constant stipulates the occurrence of atomic disorder due to the milling process. That means the grinding of the powders via high energy ball milling techniques not only reduces the crystallite size into nanoscale range (< 100 nm) but also causes in the enhancement of lattice strain. Thus, the net X-ray line broadening is due to decrease of crystallite size, development of lattice strains and also due to the instrumental effects. Normally, crystallite size is a measure of the size of a coherently diffracting domain. So, when the crystallites of the materials are <100 nm, they have very less number of parallel diffraction planes that causes broadened diffraction peaks. Similarly, the non-uniform strains arises out of heavy plastic deformation during the course of high energy mechanical milling process that causes broadening of the diffraction peaks [35].

The milling dependence of internal microstrain (e) of mechanically derived nanocrystalline -MTO powders was evaluated. The graph between $4\sin\theta/\lambda$ (taken along x-axis) and $\beta_{hkl}\cos\theta/\lambda$ (taken along y-axis) for selected diffraction peaks for

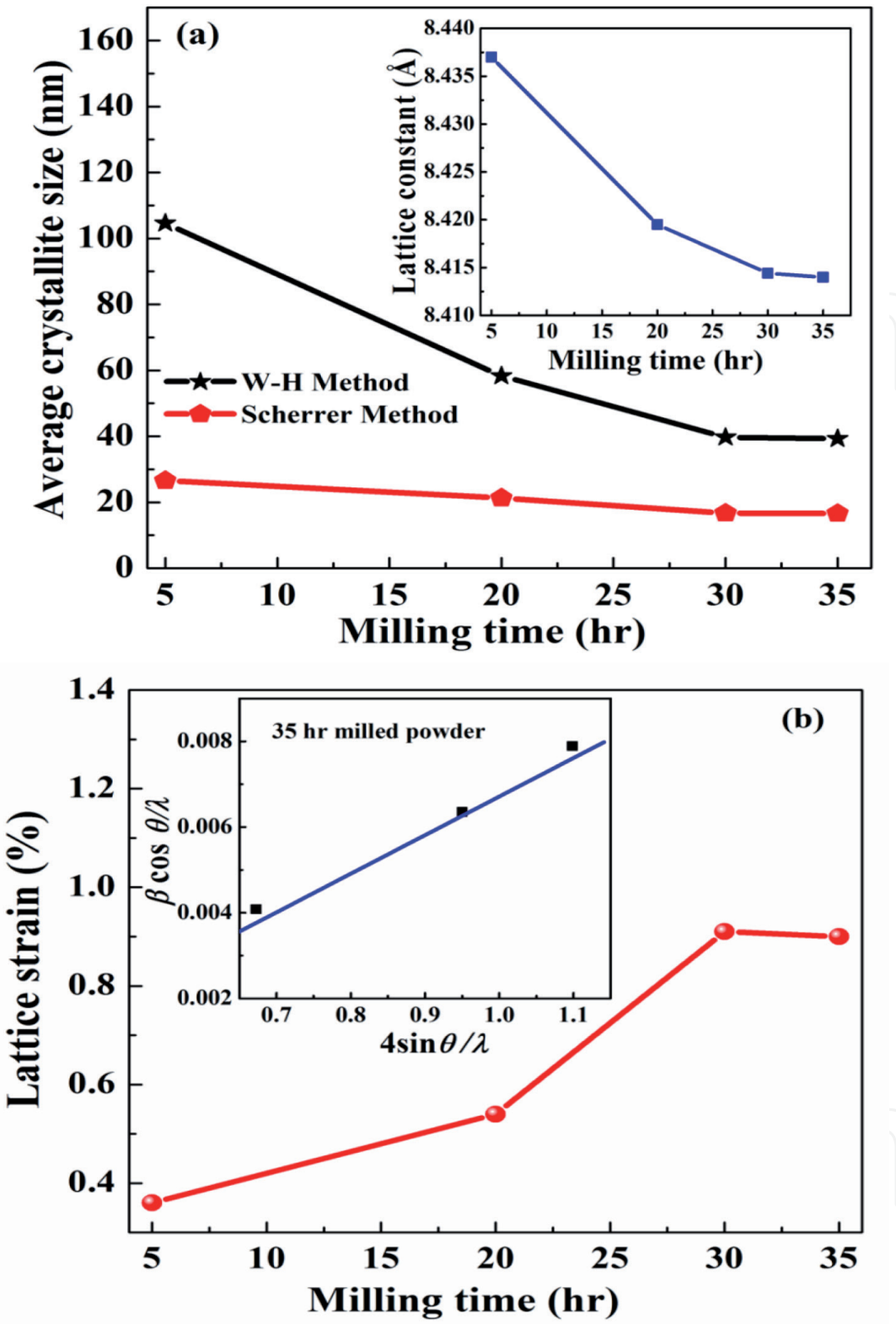

Figure 4.
*(**a**) Variations of average crystallite size and lattice parameter (**inset**) with milling time and (**b**) variation of lattice strain with milling time. **Inset:** W-H plot for 35 hrs milled powders. (adapted with permission from Bhuyan et al., 2020, @ Springer [19]).*

35 hrs milled MTO nano-powders, is plotted and is depicted in inset **Figure 4(b)**. In the present case, the crystal is considered as isotropic in nature and it is assumed that the properties of material do not depend on the direction along which it is measured. From inset **Figure 4(b)**, (called W-H plot), it shows that the data points are not much deviated from the straight line suggesting isotropic nature of

the strain. From the linear fit of the data, the average crystallite, *D* was estimated from the y-intercept and the microstrain (ε) from the slope of the fit (inset **Figure 4(b)**). For 35 hrs milled powders, the crystallite size is found to be approximately 38 nm and microstrain is around 9.01×10^{-3} respectively. Thus from the W-H analysis it is clear that the broadening of the X-ray peaks is due to the contribution of smaller crystallite size and the induction of strain. Further, it was noticed that with increase in milling duration the internal microstrain increases and it attains a constant value after a particular milling period.

3.3 Thermal analysis

In order to determine the characteristics temperature at which solid state processes are taking place, DTA and DSC analysis has been performed. **Figure 5** shows the DTA and DSC curves of the MTO system milled for 35 hrs. The initial weight loss of 6-8% was assigned to the evaporation of humidity during powder's preparation route. Around 400 -450°C, the weight loss was more prominent and apportioned to the formation of secondary phases of $MgTiO_3$ and $MgTi_2O_5$. As mechanical activation supports hygroscopy, so weight loss is the highest for the sample with the longest period of milling. So, MTO-35 has more weight loss compared with other different hours milled samples. Also, we have observed some endothermic and exothermic peaks that are related to the weight loss of the sample with temperature.

3.4 Morphological study on mechanically alloyed nanocrystalline MTO powders

3.4.1 SEM analysis

SEM micrographs were obtained to see the influence of mechanical activation on the evolution of microstructure of MTO powders milled for different hours (**Figure 6**). It is well-known that milling processes yield a significant modification in the morphology of composite materials due to severe plastic deformation of the particles during the milling process [38, 39]. Generally, the microstructure

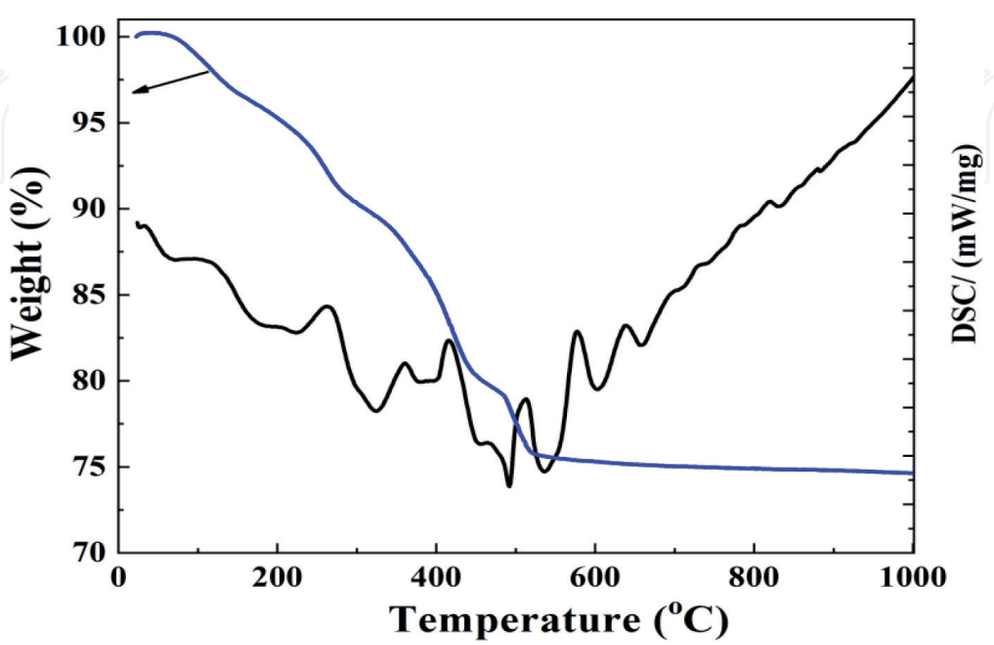

Figure 5.
TGA and DSC curves of 35 hours milled powders.

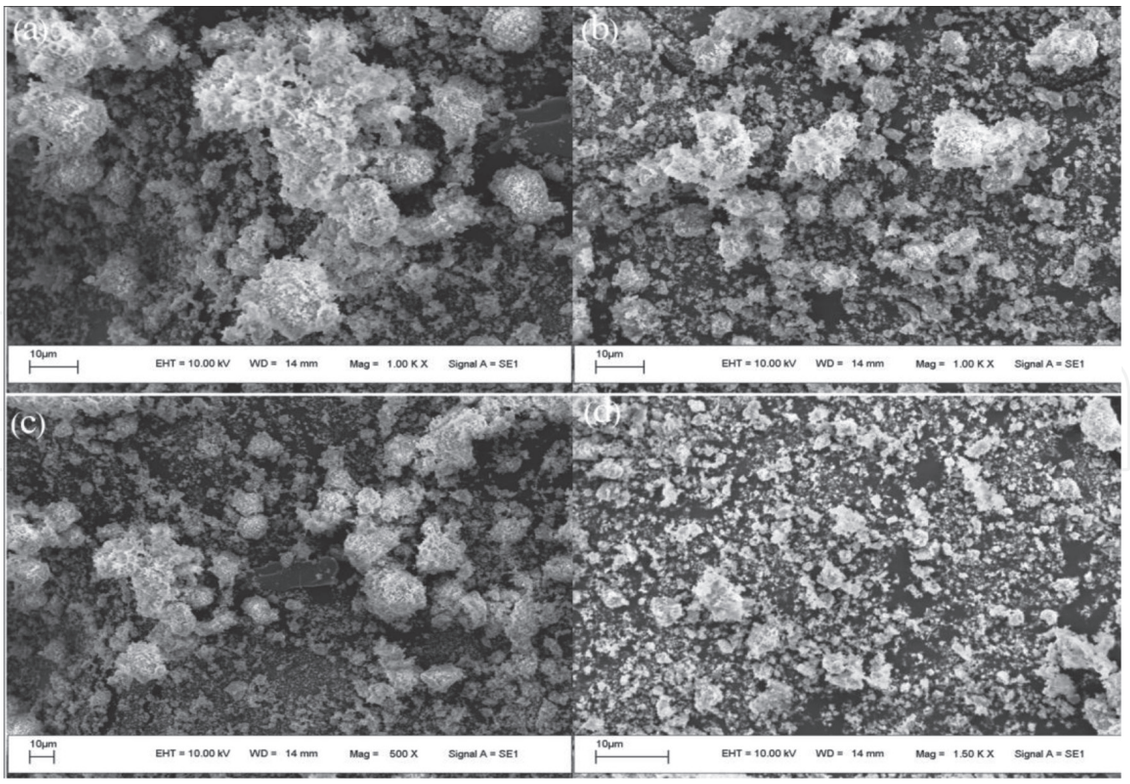

Figure 6.
SEM micrographs of the MTO powders milled for (a) 0 (b) 5 (c) 20 and (d) 35 hrs (adapted with permission from Bhuyan et al., 2020, @ Springer [19]).

evolution is controlled by the processing parameters, such as composition of the materials, rise of temperature and milling intensity. From the morphological study, it is noticed that the starting powders consists of spherical particles with extreme agglomerated morphology. After a short period of milling up to 5 hrs, there is significant effect on the morphology of the MTO powders was observed. The particles were distributed over a wide range from sub-micrometer to few micrometers with spherical in morphology. As the milling time increased up to 35 hrs, cold welding of particles was activated and the size of the particles reduced into nanometer range due to the high impact collision of the balls. At this stage more distinct granular structure particles are observed as compared to the initial stages of milling along with the presence of new phases in the shape of agglomerates covered with many smaller nanosized particles of starting powders. These clustering of MTO nanoparticles are typically mechanically alloyed powders that are resulted from repeated cold welding and fracture of powders during the process of high energy mechanical alloying. The surface morphology of the nanocrystalline MTO powders are in support as evidence to the XRD results that the crystalline nature enhances with the increase of milling durations.

3.4.2 TEM analysis

The bright field TEM images of MTO nanoparticles milled for 20 and 35 hrs are shown in **Figure 7(a)** and **(b)** respectively. From TEM images it was evident that the powders milled for 20 hrs does not exhibit that much distinct particles (clustering of MTO nanoparticles), but for 35 hrs milled powders a clear nanosized particle is observed. The size of the parent oxides is about 2 μm. As the milling time increases the size of the initial particles decreases and for 35 hrs milled nanocrystalline MTO powders the average particle size is found to be around 60–120 nm. This crystallite size is nearly consistent with the calculated data by Williamson-Hall plot method.

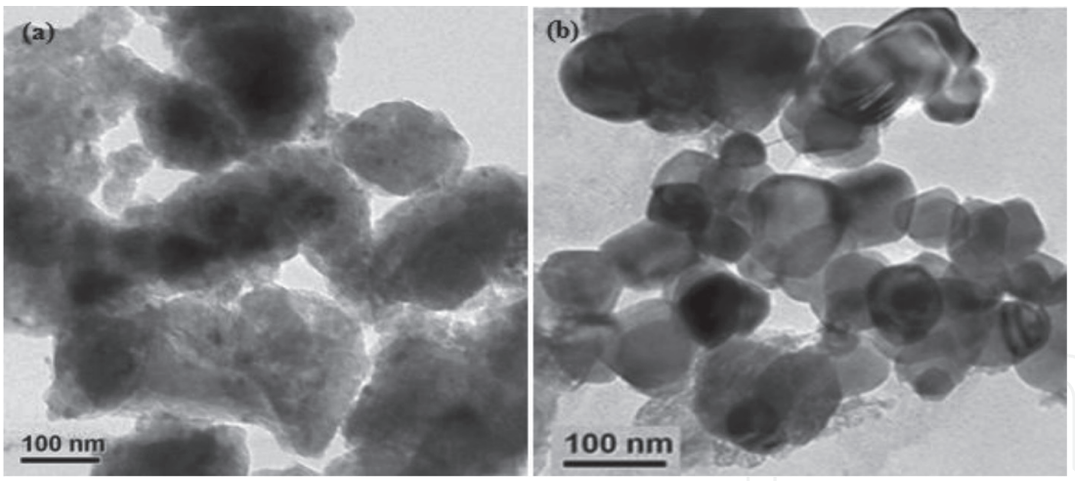

Figure 7.
Bright field-TEM micrographs of (a) 20 and (b) 35 hrs milled MTO powder.

The selected area electron diffraction (SAED) pattern of the 35 hrs milled powders is shown in **Figure 8(a)**. The SAED ring pattern indicates that the phase of MTO- nanoparticles was polycrystalline in structure and the distance between crystalline planes (i.e., inter planer spacing or *d*-spacing) was consistent with the standard pattern for a spinel MTO crystal structure. To analyze the lattice fringes for the 35 hrs milled powders, high resolution- TEM (HR-TEM) study was carried out, (as shown in **Figure 8(b)**). However, the clear lattice fringes showed that each particle has single crystalline structure. For 35 hrs milled powders, the distance between crystalline planes is evaluated and is found to 2.968 Å, which indicates the preferable crystal growth plane is (220). Thus, it could be concluded that during the high energy mechanical alloying a solid-state reaction between MgO and TiO_2 took place at room temperature.

3.4.3 Optical properties

Room temperature UV – Visible spectra were taken for all the as-prepared samples in order to see the effect of milling duration on the optical band gap of the mechanically alloyed MTO nano-powders, and are illustrated in **Figure 9**. A strong absorption peak at around 356 nm is observed for un-milled MTO powders, while with increase in milling duration, the peak slightly shifted to 352 nm for 35 hrs

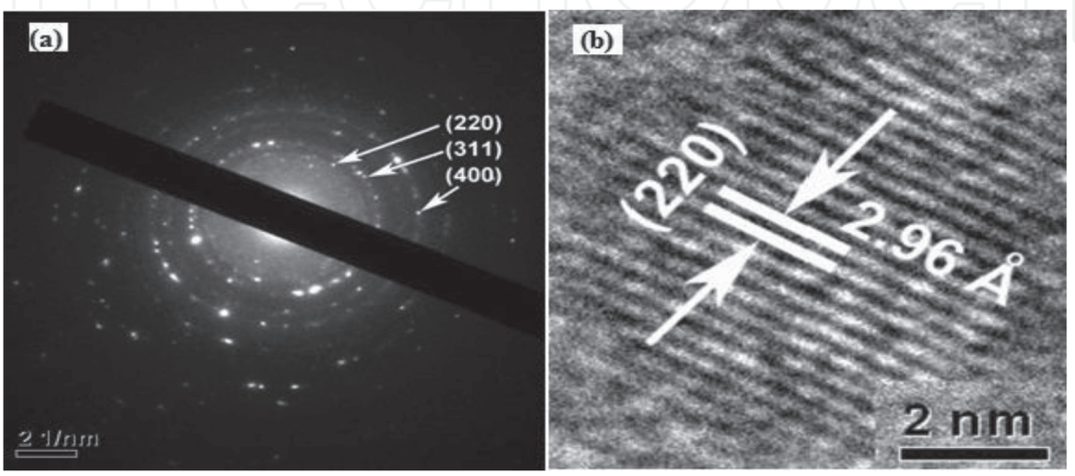

Figure 8.
(a) The selected area electron diffraction (SAED) pattern and (b) HR-TEM for 35 hrs milled powder (Adapted with permission from Bhuyan et al., 2020, @ Springer [19]).

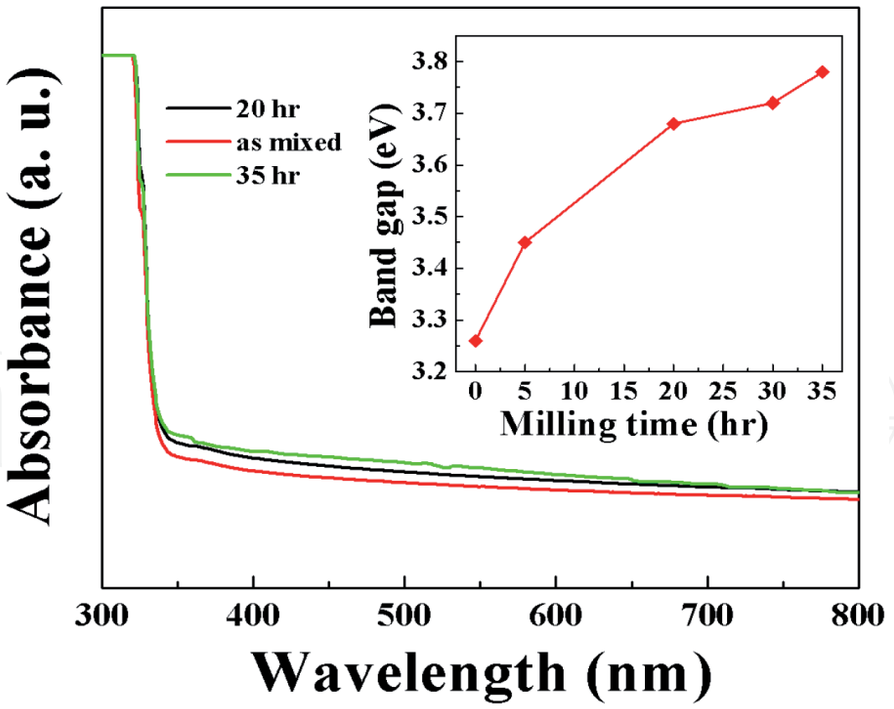

Figure 9.
Room temperature UV – Visible spectra of pure and milled MTO powders, ***inset:*** *Variation of bandgap with milling time (adapted with permission from Bhuyan et al., 2020, @ Springer [19]).*

milled powders. It shows that there is a clear sign of blue-shift in the absorption peak with decrease in average crystallite size. This indicates that with decrease in particle size the band-gap increases. However, the enhanced absorption in mechanically alloyed MTO nanoparticles can be attributed to a large surface to volume ratio and enhanced oscillator strength with decrease in average particle size.

Tauc relation [40], is employed to estimate the optical band gap of all the milled samples. According to this relation, $\alpha h\upsilon = \beta\,(h\upsilon - E_g)^{n}$, where, $h\upsilon$ is the photon energy, β is a constant which measures the crystalline order of the samples and n = 1/2 for direct bandgap structure (As MTO belongs to cubic structures and exhibiting direct band gap). The variation of bandgap with milling time is plotted and shown in inset of **Figure 9**. The plot indicates that with increasing milling time from 0 to 35 hrs the bandgap enhanced from 3.26 eV - 3.78 eV. This result is consistent with the previously reported results [40–42]. The optical bandgap (E_g) of all the milled powders are determined by the extrapolation of the best linear fit between $(\alpha h\upsilon)^2$ and $h\upsilon$ to intercept the $h\upsilon$ axis (α = 0), (taken along x-axis). The figure shows the dependence of the absorption coefficients $(\alpha h\upsilon)^2$ with photon energy. The position and slope of the optical absorption edge makes this material as a suitable UV light absorber.

4. Conclusions

Mg_2TiO_4 nanocrystalline with spinel structure were synthesized from high purity MgO and TiO_2via high energy ball milling techniques. The impact of milling time on particle size, crystal structure and the microstructure of mechanically derived Mg_2TiO_4 nanocomposite powders were investigated using X-ray diffraction, scanning electron microscopy and transmission electron microscopy (TEM) techniques respectively. Williamson-Hall method was employed to understand the origin of the broadening of the X-ray diffraction peaks. It was confirmed that the W-H method is

a more accurate method as compared to the Scherrer method for the estimation of crystallite size of the Mg_2TiO_4 nanocomposite materials. Further, the thermal decomposition behavior of the milled powders was examined by a thermo-gravimetric analyzer (TGA) in argon atmosphere. The UV–visible spectra showed strong bandgap absorption at ~356 nm and with an increase of milling times from 0 to 35 hrs, there is an increase of the band-gap from 3.68-3.78 eV. The Mg_2TiO_4 nano- powders synthesized via mechanical alloying method showed promising optical properties which is suitable for commercial optoelectronic applications. Also, the high optical absorption edge makes this material as suitable UV light absorber. Moreover, Mg_2TiO_4 is an excellent microwave dielectric material having wide band gap and high refractive index and practically useful for various optical and electronic applications.

Acknowledgements

The author RKB acknowledges Prof. Sukant Kumar Tripathy, Department of Physics, Berhampur University, Berhampur, Odisha, India for his suggestion and discussion for the betterment of the manuscript.

Author details

Ranjan Kumar Bhuyan[1*], Bhagban Kisan[2], Santosh Kumar Parida[3], Soumya Patra[4] and Sunil Kumar[5]

1 Centre of Excellence in Nanoscience and Technology for the Development of Sensor, Department of Physics, Berhampur University, Berhampur - 760007, India

2 P.G. Department of Physics, Utkal University, Vanivihar Bhubaneswar - 751004, India

3 Department of Physics, ITER, Siksha 'O' Anusandhan Deemed to be University, Bhubaneswar - 751030, India

4 School of Applied Physics, KIIT, Bhubaneswar - 751024, India

5 Department of Physics, Ramjas College, University of Delhi - 110007, India

*Address all correspondence to: ranjanphysics.bhuyan8@gmail.com

References

[1] Rabha, Susmita., Dobbidi, Pamu.; Enhanced microwave dielectric and electrical properties of Zn substituted Mg_2TiO_4 ceramics for RF/ microwave applications, *J. Mater. Sci. Mater. in Electronics,* 60, (**2019)** 392.

[2] Yu, Hongta. Luo, Ting., He, Lie., Liu Jing song.; Effect of ZnO on Mg_2TiO_4 – $MgTiO_3$- $CaTiO_3$ microwave dielectric ceramics prepared by reaction sintering route, *Adv. in Appl. Ceram.*, 118, (**2018)** 1.

[3] Kumar, T. S.; Gogoi P.; Perumal, A.; Sharma P.; Dobbidi, Pamu.; Effect of cobalt doping on the structural, microstructure and microwave dielectric properties of $MgTiO_3$ ceramics prepared by semi alkoxide precursor method, *J. Am. Ceram. Soc*., 97, (**2014)** 1054.

[4] Bhuyan, R. K.; Thatikonda, S. K.; Pamu, D.; Liquid phase effect of Bi_2O_3 additive on densification, microstructure and microwave dielectric properties of Mg_2TiO_4 ceramics. *Ferroelectrics*, 516 (2017) 173.

[5] Li, B. J.; Wang, S. Y.; Liao, Y. H.; Chen, Y. B.; Dielectric properties and crystal structure of $(Mg_{1-x}Co_x)_2(Ti_{0.95}Sn_{0.05})O_4$ ceramics. *J. Ceram. Soc. Jpn.*; 122, (**2014)** 955.

[6] Bhuyan, R. K.; Thatikonda, S. K.; Goswami, D. James, A. R.; Perumal, A.; Pamu, D.; Enhanced densification and microwave dielectric properties of Mg_2TiO_4 ceramics added with CeO_2 nanoparticles.*; Mater. Sci. Eng. B.;*178 (2013) 178.

[7] Bhuyan, R. K.; Thatikonda, S. K.; Goswami, D. James, A. R.; Pamu, D., Liquid phase effect of La_2O_3 and V_2O_5 on microwave dielectric properties of Mg_2TiO_4 ceramics. *J. Electroceramics,* 31 (2013) 48.

[8] Huang, C. L.; Chen, J. Y.; Low-loss microwave dielectric ceramics using $(Mg_{1-x}Mn_x)_2TiO_4$ (x =0.02-0.1) solid solutions. *J. Am. Ceram. Soc*., 92 (2009) 675.

[9] Huang, C. L.; Ho. C. En.; Microwave dielectric properties of $(Mg_{1-x}Ni_x)_2TiO_4$ (x =0.02-0.1) ceramics. *J. Am. Ceram. Soc*., 7(2010) E163.

[10] Cava, R. J.*;* Dielectric materials for applications in microwave communications. *J. Mater. Chem*., 11, (**2001)** 54.

[11] Huang, C. L.; Wange, J. J.; Chang, Y.P. Dielectric Properties of Low Loss (1-x) $(Mg_{0.95}Zn_{0.05})TiO_3$-$x$$SrTiO_3$ Ceramic System at Microwave Frequency, *J. Am. Ceram. Soc*., 90 (**2007)** 858.

[12] Huang, C. L.; Chen, J. Y.; Li, B. J., Effect of $CaTiO_3$ addition on microwave dielectric of Mg_2 $(Ti_{0.95}Sn_{0.05})O_4$ ceramics, *J. Alloys Compd*., 509 (**2011)** 4247.

[13] Chen, Y. B., $La(Mg_{1-x}Zn_x)_{1/2}Ti_{1/2}O_3$ ceramics at microwave frequencies. *J. Alloys Compd.*, 509 (2011) 1050.

[14] Belous, A.; Ovchar, O.; Durilin, D.; Krzmanc, M. M.; Valant, M.; Suvorov, D. High –Q microwave dielectric materials based on the spinel Mg_2TiO_4. *J. Am. Ceram. Soc*., 89 (**2006**), 3441.

[15] A. Wechsler, R. B. Von Dreele, Structure refinements of Mg2TiO4, MgTiO3 and MgTi2O5 by time-of-flight neutron powder diffraction. *Acta Cryst*., B45 (1989) 542.

[16] Kimmel G., Zabicky J., International centre for diffraction data, *Advances in X-ray analysis*. 42 (**2000**), 238.

[17] Pfaff, G.; Peroxide route for synthesis of magnesium titanate powders of various compositions. *Ceram. Int*., 20 (**1994**)111.

[18] M. Kamruddin, P. K. Ajit Kumar, R. Nithya, A. K. Tyagi, B. Raj, Synthesis of nanocrystalline ceria by thermal decomposition and soft-chemistry methods. *Scripta Materialia*, 50 (**2004**) 417.

[19] Bhuyan R. K, Mahapatra R. K, Nath G., Sahoo, B. K., Das Debadutta and D. Pamu, Influence of high energy ball milling on structural, microstructural and optical properties of Mg_2TiO_4 nanoparticles. *J. Mater. Sci. Mater. Electro.*, 31 (**2020**) 628.

[20] Bhuyan, R. K.; Thatikonda, S. K.; Pamu, D.; Structural and microwave dielectric properties of Mg_2TiO_4 ceramics synthesized by mechanical method. *Int. J. Appl. Ceram. Technol.*; 516 (**2013**) E18.

[21] Cheng, L., Peng, L., Qu, S. X., Cheng, L., Zhang, H. Wu., Microwave dielectric properties of Mg_2TiO_4 ceramics synthesized via high energy ball milling method, *J. Alloy. Compd*., 623 (**2015**) 238 .

[22] Filipovic, S., Obradovic, N., Pavlovic V. B., Markovic, S., Mitric, M., Ristic, M. M., Influence of mechanical activation on microstructure and crystal structure of sintered MgO-TiO_2 system, *Science of sintering*, 42 (**2010**) 143.

[23] H. Yang, Y. Hu, A. Tang, S. Jin, G. Qiu, Synthesis of tin oxide nanoparticles by mechanical reaction. *J. Alloy. Compd*., 363 (**2004**) 271.

[24] K. T. Paul, S. K. Satpathy, I. Manna, K. K. Chakraborty, G. B. Nando, Preparation and Characterization of Nano structured Materials from Fly Ash: A Waste from Thermal Power Stations, by High Energy Ball Milling. *Nanoscale Res. Lett*., 2 (**2007**) 397.

[25] L. B. Kong, J. Ma, W. Zhu, O. K. Tan, Preparation and characterization of PLZT ceramics using high-energy ball milling. *J. Alloys Compd*., 322 (**2001**) 290.

[26] C. Suryanarayana, *Mechanical Alloying and Milling*, Marcel Dekker, (**2004**).

[27] Rietveld, H.M.: Line profiles of neutron powder diffraction peaks for structure refinement. *Acta. Crystallogr*. 22 (**1967**) 151.

[28] Balzar, D., Ledbetter, H.J., Voigt function modeling in Fourier analysis of size and strain broadened X-ray diffraction peaks. *Appl. Crystallogr*. 26, (**1993**)97.

[29] Warren, B.E., Averbach, B. L., The effect of cold-work distorsion on X- ray pattems. *J. Appl. Phys.* 21 (**1950**) 595.

[30] Suryanarayana, C., Norton, M.G., X-ray diffraction: a practical approach. Plenum Press Publishing, New York (**1998**).

[31] Soni P. R, Mechanical alloying: Fundamental and applications, Cambridge International Science Publishing, UK (**2001**).

[32] Suryanarayana C, Mechanical alloying and milling, *Prog. Mater. Sci*. 46 (**2001**) 1-184.

[33] Koch C. C, Nanostructured materials: Processing, properties and potential applications, Noyes Publications, New York (**2002**).

[34] Ding J, Li Y, Chen L. F, Deng C.R, Shi Y, Chow Y. S, Gang T. B, Microstructure and soft magnetic properties of nanocrystalline Fe–Si powders. J. Alloys Compd. 314 (**2001**) 262.

[35] G. K. Williamson, W. H. Hall, X-ray line broadening from filed Aluminium and wolfram, *Acta Mater.*, 1 (**1953**) 22.

[36] Biju, V., Sugathan, N., Vrinda, V., Salini, S.L.: Estimation of nano crystalline silver from X-ray diffraction

line broadening. *J. Mater. Sci*. 43 (**2008**) 1175.

[37] Cullity, B.D., Stock, S.R.: Elements of X-ray diffraction, 3rd edn. Prentice Hall, New Jersey (**2001**).

[38] J. Xu, G.S. Collins, L. Peng, M. Atzmon, Deformation-assisted decomposition of unstable $Fe_{50}Cu_{50}$ solid solution during low-energy ball milling. *Acta Mater*., 47 (**1999**)1241.

[39] Bhuyan, R. K.; Pamu, D.; Sahoo B.K.; Sarangi, A. K.; Structural and thermal study of Mg_2TiO_4 nanoparticles synthesized by mechanical alloying method. *Micro and nanosystem,* 12 (**2020**) 87.

[40] J. Stade, D. Hahn, R. Dittmann, *Journal of Luminescence* 8 (**1974**) 308-317.

[41] H. Kominami, M. Tanaka, K. Hara, Y. Nakanishi, Y. Hatanaka, *Physica Status Solidi C* 3 (**2006**) 2758-2761.

[42] A. Golubovic, M. Radovic, *Journal of Serbian Chemical Society*, 76 (**2011**) 1561-1566.